Prefrontal neural ensembles encode an internal model of visual sequences and their violations

Marie E Bellet[1], Marion Gay[1], Joachim Bellet[1], Bechir Jarraya[1,2,3], Stanislas Dehaene[1,4,*], Timo van Kerkoerle[1,*] and Theofanis I Panagiotaropoulos[1,5,*]

[1]Cognitive Neuroimaging Unit, INSERM, CEA, Université Paris-Saclay, NeuroSpin center, Gif/Yvette, France

[2]University of Versailles Saint-Quentin-en-Yvelines, Université Paris-Saclay, Versailles, France

[3]Neuromodulation Unit, Foch Hospital, Suresnes, France

[4]Collège de France, Université Paris-Sciences-Lettres (PSL), Paris, France

[5]Lead Contact

Correspondence: marie.bellet@cea.fr, theofanis.panagiotaropoulos@cea.fr

*These authors jointly supervised this work.

Abstract

Theories of predictive coding hypothesize that cortical networks learn internal models of environmental regularities to generate expectations that are constantly compared with sensory inputs. The prefrontal cortex (PFC) is thought to be critical for predictive coding. Here, we show how prefrontal neuronal ensembles encode a detailed internal model of sequences of visual events and their violations. We recorded PFC ensembles in a visual "local-global" sequence paradigm probing low and higher-order predictions and mismatches. PFC ensembles formed distributed, overlapping representations for all aspects of the dynamically unfolding sequences, including information about image identity as well as abstract information about ordinal position, anticipated sequence pattern, mismatches to local and global structure, and model updates. Model and mismatch signals were mixed in the same ensembles, suggesting a revision of predictive processing models that consider segregated processing. We conclude that overlapping prefrontal ensembles may collectively encode all aspects of an ongoing visual experience, including anticipation, perception, and surprise.

Introduction

A central function generally ascribed to the primate prefrontal cortex (PFC) is the generation, maintenance and flexible use of representations and schemas, including abstract rules, in order to guide behavior and facilitate cognitive control (Miller and Cohen, 2001; Wallis et al., 2001). Within the theoretical framework of predictive coding, these prefrontal representations can be conceptualized as internal models that generate predictions onto the external world (Euler, 2018; Meirhaeghe et al., 2021; Pinotsis et al., 2019; Summerfield et al., 2006, 2008). Assemblies of PFC neurons would form abstract internal models of the statistical regularities that are frequently encountered in the environment, and use these models to project predictions that guide decisions and facilitate sensory processing (Dehaene et al., 2015; Friston, 2005; Summerfield and de Lange, 2014). Although the neuronal correlates of cognitive control and decision processes have been extensively studied in the primate PFC (Mante et al., 2013; Markowitz et al., 2015; Merten and Nieder, 2012; Miller et al., 1996; Siegel et al., 2015; Stokes et al., 2013), the implementation of internal models and predictive coding computations in PFC ensembles has not been yet characterized at the cell assembly level, but only inferred indirectly from macroscopic brain signals, particularly responses to sequence violations (Chao et al., 2018; Gil-da-Costa et al., 2013; Uhrig et al., 2014; Wang et al., 2015; Wilson et al., 2017).

In predictive coding models, indeed, the incongruence of sensory information with an already established internal model results in a surprise signal that serves to update the model (Friston, 2010). Based on this theoretical framework, deviations from learned stimulus sequences of variable complexity have been used to probe the respective complexity of predictive representations in the brain, showing that

these models unfold at multiple hierarchical scales, reflecting different levels of abstraction and engaging different cortical areas (Dehaene et al., 2015).

The most commonly studied brain signal to sequence deviants is the mismatch negativity (MMN; Näätänen et al., 1978). In the classical auditory oddball paradigm, a local regularity is established by the repetition of one tone, which leads to a reduction in brain responses; at this point, the presentation of a rare (deviant) tone yields the MMN signal, a stronger negative deflection of the scalp EEG compared to repeated stimuli (for a review see Näätänen et al., 2007). Although feed-forward adaptation may contribute to the MMN (Garrido et al., 2009; May and Tiitinen, 2010), several results indicate that it, and similar visual violation responses (Pazo-Alvarez et al., 2003) primarily reflects predictive processing (Garrido et al., 2009; Summerfield et al., 2008; Wacongne et al., 2012; Winkler, 2007). The source of auditory MMN has been localized in the secondary auditory cortex, superior temporal gyrus and PFC (Deouell, 2007; Dürschmid et al., 2016; Shalgi and Deouell, 2007).

The primate brain does not stop at encoding repetitions, however. Multiple paradigms indicate that non-human primates can infer sequence regularities at a more temporally extended and abstract level, for instance the extraction of the same pattern from sequences comprised from different stimuli (e.g. AAB and CCD) (Wang et al., 2015). Processing such higher-order sequential structures necessarily abstracts away from the specific stimulus identities and may therefore engage higher-order associational cortical areas, in particular the PFC.

We have previously studied these two levels of sequence processing using a hierarchical “local-global” sequence paradigm where auditory stimuli are presented in short sequences. During an entire block, all sequences follow the

same pattern, either 4 repeats of the same stimulus (e.g AAAA), or 3 repeats followed by a deviant (e.g. AAAB). Following the repeated presentation of one of these global sequence patterns, the ability to detect global violations is probed by presenting sequences that deviate from the pattern (AAAB or AAAA, respectively; global deviants). In contrast to the MMN, mismatch responses to such global deviants are delayed, require consciousness, and predominantly arise from higher-order cortical areas of humans and macaques (Bekinschtein et al., 2009; Chao et al., 2018; El Karoui et al., 2015; Uhrig et al., 2014), including the ventrolateral prefrontal cortex (vlPFC). Intracranial recordings of global field potentials indicate that PFC sends feedback signals to upstream cortical areas after the violation of global sequence expectations (Chao et al., 2018).

From the observation of such mismatch signals, it was indirectly inferred that the PFC and associated high-level areas comprise an internal model of the ongoing sequences. Here, we tested this idea directly by recording from PFC neuronal ensembles during a visual version of the “local-global” test. We asked two questions. First, do PFC neurons encode all aspects of the sequences in the local-global paradigm, therefore holding a complete internal model of the ongoing sensory stream and its occasional violations? Second, are these neural representations abstract, independent of the specific stimulus identities used to convey the sequence pattern, as predicted by earlier work (Wang et al., 2015)?

We tested these hypotheses by recording from chronic multielectrode arrays in macaque vlPFC during a local-global paradigm with visual stimuli. Using multivariate decoders, we show that prefrontal neuronal populations encoded, within distinct neural subspaces, all aspects of the visual sequences, including image identity, serial position of stimuli, global context and local and global

structure violations. Global sequence context and its mismatches could be traced to the same population subspace, indicating an integrative level of predictive processing in the PFC. Furthermore, local mismatch responses could not be fully explained by stimulus-specific adaptation (SSA), but reflected genuine deviance detection. These neuronal representations generalized between sequences with different image identities, suggesting that prefrontal ensembles comprise an abstract internal model of visual sequence patterns.

Results

vlPFC spiking activity during the visual local-global paradigm

We recorded spiking activity with multielectrode Utah arrays, chronically implanted in the vlPFC of two macaque monkeys (Fig. 1A), during exposure to the local-global paradigm (Bekinschtein et al., 2009) with visual stimuli (Fig. 1B-D). In order to eliminate confounding activity related to decision making and motor responding, the task did not require overt behavioral report, but mere sequence observation. For completion of a trial, the monkeys received a liquid reward at 100 ms after offset of a sequence. On each trial, a sequence of 4 images (300 ms stimulus duration; 300 ms inter-stimulus interval) was presented on a screen while the monkeys maintained the gaze within the image region (Fig. 1B). A sequence consisted either of 4 repeats of the same stimulus (xxxx sequence, from hereon abbreviated as xx) or of 3 repeats and one *local deviant* in the last position (xxxY sequence, abbreviated as xY; Fig. 1C). These sequences were embedded in blocks of 200 trials where one sequence type (xx or xY) was the frequent sequence (global standard). The animals were habituated to the global standard sequence during the first 50 trials of each block. Of the remaining 150 test trials,

80% were global standards and 20% were global deviants, which differed only in the last position compared to the standard. We will use a notation that indicates trials according to their local structure and global context: e.g. a rare xY trial (in an xx block) will be denoted as xY|xx. The first two letters indicate the current trial and the last two letters the global context in which it occurred (Table 1).

In each recording session, a specific pair of images (A and B) was chosen, out of five possible pairs (Fig. 1C,D), and 4 blocks were run with this picture pair, in random order (two xx blocks, aa and bb; and two xY blocks, aB and bA). This allowed us to test whether neural representations of sequence structure generalized across stimulus identities within and across sessions. Indeed, the design enabled us to distinguish effects of first-order (local) versus higher-order (global) sequence regularity, which require representing the whole sequence pattern (Methods).

The recorded multi-unit activity (MUA), i.e. the sum of recorded spikes from each electrode, was robust over several days in both animals, with overall more active sites in monkey A. First, for consistency with prior research with global brain-imaging signals (Basirat et al., 2014; Bekinschtein et al., 2009; El Karoui et al., 2015; Uhrig et al., 2014), we assessed the univariate responses to local and global violations. Within individual recording sites, we first examined the MUA in response to “pure” local deviance (frequent xY vs. frequent xx trials) and compared them to the effects of “pure global” deviance (rare xx vs. frequent xx). The rank sum statistics provided a measure of the size of the effects of local and global deviance for each channel (Fig. 2A). After controlling for multiple comparisons, about half of the channels revealed a significant response to local

deviance, and ~ 3 % or 0.8 % to global deviance, in monkey A or H, respectively (Fig. 2B).

The inspection of the peri-stimulus time histogram (PSTH) from individual channels provided insight into the variety of neural response types (Fig. 2C). Many sites responded strongly to local violations (Fig. 2C left), with a very large firing response to the last image Y in xxxY trials that exceeded the response to any of the previous images. At some but not all sites, this response was modulated by context, and was reduced for predicted local deviants (xY|xY; Fig. 2C, bottom left). Finally, several sites showed distinct firing as a function of global context (xx or xY blocks), already during the first three stimuli of a sequence, and a change in firing when a "pure global deviant" occurred (Fig. 2C, top right).

VLPFC ensembles form a rich representation of visual sequences

Given the diversity of response types and signs of mixed selectivity, we hypothesized that visual sequences could be better represented as neuronal population vectors rather than within individually specialized neurons, as suggested by others for PFC (Baeg et al., 2003; Ebitz and Hayden, 2021; Mante et al., 2013; Parthasarathy et al., 2017; Rigotti et al., 2013) We used regression analyses to test whether vlPFC represented all the variables that defined the visual sequences in the local-global paradigm, namely (i) *stimulus identity* (1 of 2 possible images in each session), (ii) *serial position* of the image within each sequence (from 1 to 4) (iii) *global context* (xx or xY block), (iv) *local deviance*, and (v) *global deviance.* For this analysis, we used only the data from the test trials that followed the first 50 habituation trials in each block, to ensure that the current global context could be learned (see also Fig. 4 G,H). We applied multivariate

linear regression for all variables but serial position, for which we used multinomial logistic regression (Methods). This approach allowed us to determine which population vectors, if any, carried maximum information about each sequence variable. These vectors were then used to reduce the dimensionality of the MUA and obtain trajectories of the neural population within each neural subspace (Fig. 3). Using the subspace trajectories for classification allowed us to decode each of the sequence variables. Such decoding, relative to chance level, was quantified using the area under the receiver operating characteristic curve AUROC (see Fig. S1 for Methods).

The results showed that all variables could be decoded at above-chance levels (Fig. 3). First, the decoding performance for stimulus identity (image A vs. B within each recording session) was close to 1 for every item in a sequence, including the last sequence item when it changed on xY trials (Fig. 3A,F). Thus, vlPFC populations robustly encoded the visual stimuli throughout the entire trial. Second, using a separate decoder for serial position within a sequence, we could predict ordinal position from neuronal population activity, particularly for the first and last items, but also at above-chance levels for ordinal positions 2 and 3 (Fig. 3B,F, predictions are indicated by horizontal bars). Note that, because the sequences used a fixed timing, ordinal decoding could be due to numerical codes, temporal codes or both (see Kapoor et al., 2018; Nieder, 2012). However, elapsed time alone could not explain all of the findings, such as the fact that the code for "1st item" was partially reactivated for the last image of xY trials (the first image with this identity); or that the code for "4th item" was reactivated at ordinal positions 1, 2 or 3 on trials when the monkey broke fixation and the visual sequence was aborted, suggesting that it actually responded to "last item" (Fig. S2). These

findings indicate that those neural codes were partially locked to the phase of the task, and not solely to item number or timing.

Third, to test whether vlPFC neurons contained a model of the upcoming sequence structure, we decoded the global context (xx or xY block) from the neuronal population activity prior to the last stimulus of a sequence. We indeed identified a population subspace whose activity allowed us to infer the global context even before the sequence started (Fig. 3C,H). Thus, vlPFC populations represented the sequence that recurred in a given block prior to sequence presentation, and not just prior to or after the local deviant. Below, we will look in more detail at the properties of this neural subspace and how it builds up during the habituation period.

Fourth, we assessed the presence of responses to violations of either local or global sequence regularity. The population that was sensitive to local deviance showed a response to both predicted and unpredicted local deviants (Fig. 3D,I orange and yellow). Decoding local deviance was almost perfect on a single-trial basis, with an early peak (~200 ms), indicating a very robust and fast response to local novelty. Nevertheless, the activation was stronger upon unpredicted than predicted local deviants, in agreement with the predictive coding framework (Fig. S4). Global deviance (rare versus frequent sequences in a given block) could also be decoded with a later peak (~500 ms after last item onset). In contrast to the unimodal phasic response observed for local deviants, the trajectories of the population encoding global deviance showed a bi-phasic response. First, until around 300 ms (200 ms in monkey H) following the last stimulus onset, only trials with a local deviant showed a positive activation (Fig. 3E,J orange and yellow), again with a higher amplitude for unpredicted local deviants. However, in a later

phase, after 300ms, both types of rare trials (xY|xx and xx|xY) evoked a response into the same direction (yellow and cyan), and opposite to the frequent trials (orange and blue). We separately measured the global deviance decoding performance by computing the AUROC for rare vs. frequent xY (Fig. S3 A,B dashed) and rare vs. frequent xx trials (Fig. S3 A,B solid). This analysis confirmed that an early response to global deviants was only present for rare xY trials and a later mismatch response was present for both sequence types, thus reflecting abstract global deviance detection invariant for sequence pattern. To further probe such abstraction, we evaluated a “cross-condition” decoder trained on xx trials and tested on xY trials (Fig. S3 C,D). Generalization across the two sequence structures only occurred late after the last item onset (~300-500 ms), indicating that by that time the neural code for global surprise was shared by the two sequences with a different local structure. This finding also suggests that the neural subpopulation coding for global deviance might be largely segregated from the subpopulation coding earlier for local deviance. We assessed the independence of these two neural populations by decoding global deviance from the subspace that represented local deviance and found that the late global mismatch response was indeed not encoded in the subspace that showed a late local mismatch response (Fig. S4). Importantly, neural deviance responses could not be explained by the generation of eye movements, which were found to be a behavioural read-out of local novelty detection (Fig. S5). The different time scales of the local and global effect are consistent with previous results, showing that the processing of global sequence violations requires longer times for conscious integration compared to the detection of local deviants (Bekinschtein et al., 2009; Strauss et al., 2015; Wacongne et al., 2011).

Altogether, those findings indicate that the vlPFC population that we sampled comprised multiple, overlapping and distributed representations of all the features of our visual sequences.

The representation of global context is learned during habituation and updated by errors

We next examined how the neural activity within the subspace that represented global context (xx or xY sequence) was updated. Predictive coding models should predict that, following a global violation, the internal model should be destabilized or updated, at least transiently. Thus, Figure 4 A,B shows neural activity project on the global context axis, depending on both the context (xx or xY) and the preceding trial (global standard or global deviant), prior to and during the presentation of the first 3 sequence items. In both monkeys, there was sustained activity persisting throughout all trials and distinguishing xx from xY context, regardless of the previous trial (Fig. 4C,D). A trial in an xY block, for example, led to an activation into the "xY-direction" of this subspace during the first three stimuli in a sequence, whether following a global standard xY|xY (Fig. 4A,B orange solid) or a global deviant xx|xY trial (Fig. 4A,B orange dashed). This observation is important as it indicates that the activity was not simply due to a lingering memory of the previous trial, but was sustained in the long term, as needed to encode the global context of an entire session. Nevertheless, the encoding strength of global context was reduced after the occurrence of a global deviant (Fig. 4 A,B dashed vs. solid). This effect was transient, and activity was quickly restored in the following trials (Fig. 4E,F).

We also examined how this activity was built up during the first 50 habituation trials of a block (Fig. 4 G,H). The divergence between xx and xY blocks was present early on, within the first 10 presentations of a given sequence, but it continued to increase continuously through the habituation period of 50 trials. Together, these two findings show that the context was inferred at a long time scale by this neural population, but modulated by global errors on a shorter time scale. The first finding reflects the emergence of an expectation about the global regularity in vlPFC, while the latter fits with a transient destabilization or update of this model after a global mismatch.

A shared code for global deviance and context

Current models of predictive coding hypothesize that at each level of the cortical hierarchy separate neural populations code for predictions and prediction errors (for a review Walsh et al., 2020). Thus, expectation and error signals might occur in completely segregated ensembles. Alternatively, the representation of context might happen within the same neural population, which also emits the mismatch responses. To address this issue, we studied the overlap of deviant and context responses in PFC. To do so, we projected the unfolding population MUA onto the vector corresponding to maximal global deviance decoding performance (+- 100 ms around the maximum time bin) (Fig. 4I,J). We found that the resulting population trajectories also segregated as a function of the global context, i.e. xx versus xY blocks (Fig. 4I,J). During the first three items, there was a slightly larger activation into the direction of global deviance on xY blocks than on xx blocks. This was reflected by a significant AUROC for context decoding from these trajectories (Fig. 4I,J bottom). It is important to note that, conversely, this effect of

context cannot entirely explain the deviance response to rare xx trials, because the latter elicited an additional increase in activity after the last stimulus (Fig. 4 I,J top cyan). We can hence conclude that parts of the neural code for global deviance detection was shared with the representation of global context.

Representation of sequence structure generalizes across stimulus identities

The above results establish that vlPFC contains partially independent neural representations of global context, local deviance, and global deviance. Furthermore, the above analyses were applied across the two pictures that were presented in a given session (A and B), hinting at the existence of neural codes that generalize across stimulus identities. To further test this point, we exploited the chronic nature of recordings and tested the generalization of the population codes across sessions with the same or different stimulus pair, always presented on different days. We found that the same neural representations allowed us to decode global context, local deviants, and global deviants, respectively, even for stimulus pairs that were different from the one presented in the training session (Fig. 5). This indicates that vlPFC sequence representations were stable for multiple days and held across several image identities, possibly reflecting an abstract neural code.

Rather than a difference between predicted and seen pictures, the representation of local deviance could however reflect the indirect effect, on vlPFC, of stimulus-specific adaptation (SSA) occurring at an earlier stage such as inferotemporal cortex (IT). Neural responses would be smaller on BBBB trials than on AAAB trials because the response to picture B would have been adapted (Garrido et al., 2009; May and Tiitinen, 2010). Note that SSA in IT is picture-specific (Meyer and Olson,

2011), but if the signal from multiple picture-specific neurons in IT was integrated in vlPFC, it would explain the observed generalization across different pictures. To test whether the vlPFC population response to local deviants reflected genuine deviance detection or merely SSA, we performed an additional experiment in monkey A, presenting new random sequences with different numbers of image repetitions and changes (Figure 6A, letters indicate any of >900 images). Contrasting the activation evoked by the last stimulus in XXXY sequences with the last stimulus in WXYZ sequences allowed us to disentangle deviance and SSA, as done with the many-standards control in the MMN literature (Ruhnau et al., 2012): deviance detection predicts a novelty response to XXXY (where a prediction develops about X), but none to the unpredictable sequence WXYZ, as the image identity of each item changed on every trial; SSA, however predicts no difference, as the last picture is equally novel and non-adapted in both cases. The results supported deviance detection (see direction of activation in Fig. 6A and decoding performance in Fig. 6B): local deviants always led to a larger response of this neural subpopulation (Fig. 6C; Fig. S6) indicating that vlPFC indeed encodes deviance from a local context, regardless of picture identity. Indeed, we found that MUA responses underlying this neural subspace were far more diverse than what would be expected based on the adaptation hypothesis (Fig. 6D), namely a simple decrease in response amplitude upon repetition. This strongly suggests that PFC populations encode sequence deviance in an abstract way: as previously inferred indirectly through brain-imaging signals (Wang et al., 2015), PFC populations signal that “the last sequence item was different from the three preceding ones”.

Discussion

Using a visual version of the local-global paradigm, we demonstrated that neuronal ensembles in macaque prefrontal cortex encode not only the concrete picture identity but also all other abstract aspects of visual sequences, such as the ordinal position of each picture and/or task phase, the global sequence pattern (xx or xY) which was repeatedly presented on a given block, and whether the current sequence comprised local and global violations. Those results show that PFC neurons encode an internal model of the various aspects of a perceived visual sequence. They concur with previous studies showing that prefrontal populations encode rich information about image identity, sequential order, ordinal number, context and task-relevant information (Donahue and Lee, 2015; Fujii and Graybiel, 2003; Kim and Shadlen, 1999; Mante et al., 2013; Miller et al., 1996; Nieder and Merten, 2007; Rigotti et al., 2013; Saez et al., 2015; Viswanathan and Nieder, 2013; Watanabe and Sakagami, 2007) even in the absence of any task requirement or active report (Kapoor et al., 2018; Panagiotaropoulos et al., 2012; Wang et al., 2015).

Overlap of global context and error representations

Theories of Bayesian predictive processing suggest that perception is an inferential process performed by cortical networks at multiple stages of the cortical hierarchy. A central hypothesis of these models is a functional segregation of prediction and error representations, namely different neuronal populations representing internal models or expectations about sensory input and their update, respectively (Bastos et al., 2012; Friston, 2010, 2018; Rao and Ballard, 1999; Walsh et al., 2020). Our results confirm the existence of local and global error

signals in PFC, as predicted by the theory and in agreement with macroscopic signals recorded with EcoG in the primate brain (e.g. Chao et al., 2018; Dürschmid et al., 2019). Frontal cortical areas have also been shown to provide contextual information in the rodent V1 (Hamm et al., 2021), possibly through gain modulation of neuronal activity (Zhang et al. 2021). Howeverr, in our recordings, contextual and violation signals were coded by activity vectors intermingled within the same neural population. Furthermore, the prefrontal neural population that emitted abstract pure global responses to deviations from a learned sequence also represented the global context. This convergence of predictive coding computations at the population level may be a particular feature of PFC neurons, which are known for their role in integrative processes and mixed selectivity properties (Parthasarathy et al., 2017; Rigotti et al., 2013). Interestingly, axons from the anterior cingulate cortex, a medial frontal cortical area, projecting to V1 in the rodent brain were not found to be modulated by deviant stimuli (Hamm et al., 2021). This discrepancy might point to a different role of the primate PFC, where we found responses to deviant stimuli, compared to rodent frontal cortex. Alternatively, this could indicate a functional specialization of primate frontal cortical areas, with the vlPFC more likely to reflect both types of responses (deviant and context). It is worth noting that in an auditory oddball paradigm, context-dependent mismatch responses were indeed observed in rat PFC (Casado-Román et al., 2020). Since we performed a population analysis, it is unclear to what degree specific single neurons process exclusively predictions or errors. It is also currently unclear whether such a segregation exists in other than the vlPFC prefrontal areas or in different layers of the PFC. However, the

detection of this overlap in our vlPFC recordings strongly suggests a convergence of these two computations in prefrontal cortex.

Abstract sequence processing in the vlPFC

In the mouse primary visual cortex, neurons perform deviance detection in correlation with feature (i.e. orientation) selectivity (Hamm et al., 2021). Therefore, different V1 neurons respond to deviant stimuli depending on their tuning. The same holds true in the auditory cortex of the rat where error responses were found to be strongly driven by the spectral characteristics of auditory stimulation (Casado-Román et al., 2020). Likewise, in monkey IT, neurons respond to unexpected pictures in a stimulus-specific manner (Meyer and Olson, 2011; Meyer et al., 2014) that can be explained by adaptation to repeated pictures (Kaliukhovich and Vogels, 2014; Miller et al., 1991). By contrast, our findings suggest that in the macaque vlPFC, both low- and high-level mismatch responses and context representations are generalized across different sets of visual stimuli, suggesting an abstract code.

Interestingly, in contrast to previous studies (Camalier et al., 2019) stimulus identity could also be decoded in vlPFC. Those results suggest that vlPFC has access to both concrete information as well as to abstract sequence structures. The abstract nature of processing reflected in context and mismatch responses could be a feature of higher-order associative cortical areas, suggesting a differentiation of predictive-processing computations compared to sensory cortical areas. Indeed, in the macaque temporal lobe, prediction errors in the middle lateral (ML) face patch reflect a higher-order tuning that may cascade from the hierarchically higher anterior medial (AM) face patch in a top-down manner,

compatible with a top-down feedback of prediction errors (Schwiedrzik and Freiwald, 2017). The current evidence, although still sparse, supports a hierarchical picture of predictive computations (Friston, 2005; Wacongne et al., 2011), where abstract predictions arise from associational cortical areas while item- and feature-specific predictions occur in sensory cortices.

Local deviance responses fit in a predictive coding framework

We identified a neural subspace that represented local deviants (mismatches) and which generalized across days and image identities. There is an ongoing controversy about the mechanisms of such mismatch detection (Auksztulewicz and Friston, 2016; Carbajal and Malmierca, 2018; Garrido et al., 2009; May and Tiitinen, 2010; Todorovic and Lange, 2012). Such a response could stem from two distinct mechanisms: a higher-order process of prediction error, with an active neural response representing the violation of a top-down prediction (Casado-Román et al., 2020; Chao et al., 2018; Hamm et al., 2021; Parras et al., 2017; Summerfield et al., 2008), or alternatively, a passive feedforward process of stimulus-specific adaptation (Fishman and Steinschneider, 2012; Kaliukhovich and Vogels, 2014; May and Tiitinen, 2010). Here, in a control experiment, we provide strong support of the predictive coding framework by showing how a rare local deviant (last stimulus in XXXY trials) elicited a stronger population response than an equally rare stimulus that was not preceded by a local regularity (WXYZ trials; Fig. 6). In both conditions, the first three stimuli in the sequence were different from the last stimulus, which makes this result difficult to explain by stimulus-specific adaptation. Further studies using parametrically-controlled stimuli and

neural tuning measurements could provide a full picture of the independence of deviance responses from stimulus-specific adaptation.

Under the assumption of hierarchical predictive processing, it could seem surprising that local deviance effects were so strongly represented in vlPFC. In the local-global paradigm, a response to local deviance (xY stimulus) is normal on xx blocks. However, we also found a strong response to predicted local deviants, i.e. when the xY stimulus occurred repeatedly and became the expected global standard sequence. This suggests that bottom-up prediction error signals remain present in the vlPFC and are not fully (or not immediately) compensated for by a top-down prediction. In support of this idea, the neural population responses in Figure 4I,J exhibit a transient local deviance response, followed a few hundreds of milliseconds later by a response to global deviance. We suggest that local deviance constitutes an important and salient feature of the local-global task to which monkeys paid attention, thus leading to its strong representation in the PFC. Importantly, inferring the global context would not be possible without a knowledge of local deviance. Hence, and although this may seem in contrast to theoretical models of predictive coding, it makes sense that PFC encodes local as well as global error signals. The fact that these responses generalize across images points to the high-level nature of sequence representations in vlPFC. A previous study, using fMRI, concluded that monkey PFC must comprise distinct representations for the number of items in a sequence (numerosity knowledge) and for the fact that the last item was identical to or different from the previous ones (sequence knowledge), regardless of the specific auditory stimuli used to convey those concepts (Wang et al., 2015). The present results fully confirm those conclusions with a more direct recording method.

Perceptual inference and consciousness

It has been suggested that PFC participates in a global neuronal workspace (GNW) critical for conscious access (Dehaene and Changeux, 2011; Dehaene et al., 1998). Indeed, the contents of visual consciousness can be decoded from prefrontal neuronal activity and PFC signals whether a stimulus was or was not consciously perceived (Kapoor et al., 2018; Levinson et al., 2021; Panagiotaropoulos et al., 2012; van Vugt et al., 2018). The present results are congruent with the GNW hypothesis since they indicate that, in the awake monkey, PFC contains superimposed neural codes for all of the concrete and abstract features of the perceived visual sequences. Some of these features encode expectations of the upcoming sequence, a finding which fits with prior evidence that PFC anticipatory signals may be critical for detecting perceptual ambiguity and biasing conscious perception through ongoing fluctuations (Kapoor et al., 2020; Moutard et al., 2015; van Vugt et al., 2018) or the provision of perceptual hypotheses (Summerfield et al., 2008; Weilnhammer et al. 2021). Our results showing decoding of context from prefrontal populations indeed suggest a strong influence of expectation in the activity of prefrontal ensembles.

Conclusion

We detected candidate signals of predictive processing in the macaque PFC that were characterized by integration, abstraction and error detection. Those signals reveal that macaque monkeys, even in the absence of overt behavior, encode visual sequences at multiple levels, including abstract neural codes for ordinal position and/or task phase and sequence pattern, regardless of the particular images used. In this respect, the present results confirm that a representation of

algebraic patterns such as xxxY ("4 items, the last of which is different") is accessible to non-human primates (Dehaene et al., 2015). Most importantly, it provides insight into the neural code for sequences, which relies on a superimposition of multiple vector subspaces, each representing a specific dimension of the perceived sequence. Finally, we showed how these representations can be updated by low- and high-level deviance detection mechanisms. It remains to be shown whether and how these PFC signals influence downstream or upstream cortical areas. Future studies, recording simultaneously from multiple cortical areas and using laminar recordings, will be needed to probe how inter-areal exchanges contribute to predictive processing.

Acknowledgements

We thank Julien Lemaitre for providing veterinary care, Abhilash Dwarakanath for his help with the data preprocessing pipeline and Pierre-Louis Bellet for providing the brain graphic of Figure 1. This project/research has received funding from the European Union's Horizon 2020 Framework Programme for Research and Innovation under the Specific Grant Agreement No. 945539 (Human Brain Project SGA3).

Author contributions

Conceptualization: M.E.B., B.J., T.v.K., T.I.P., S.D., Experimental design: T.v.K. and T.I.P., Analyses: M.E.B, Data acquisition: M.G., T.I.P, Control experiment design: M.E.B and J.B., Control experiment data collection: J.B., Surgery: M.G.,

B.J. and T.I.P., Manuscript writing: M.E.B, T.v.K, S.D. and T.I.P, Visualization: M.E.B

Declaration of interests

The authors declare no competing interests.

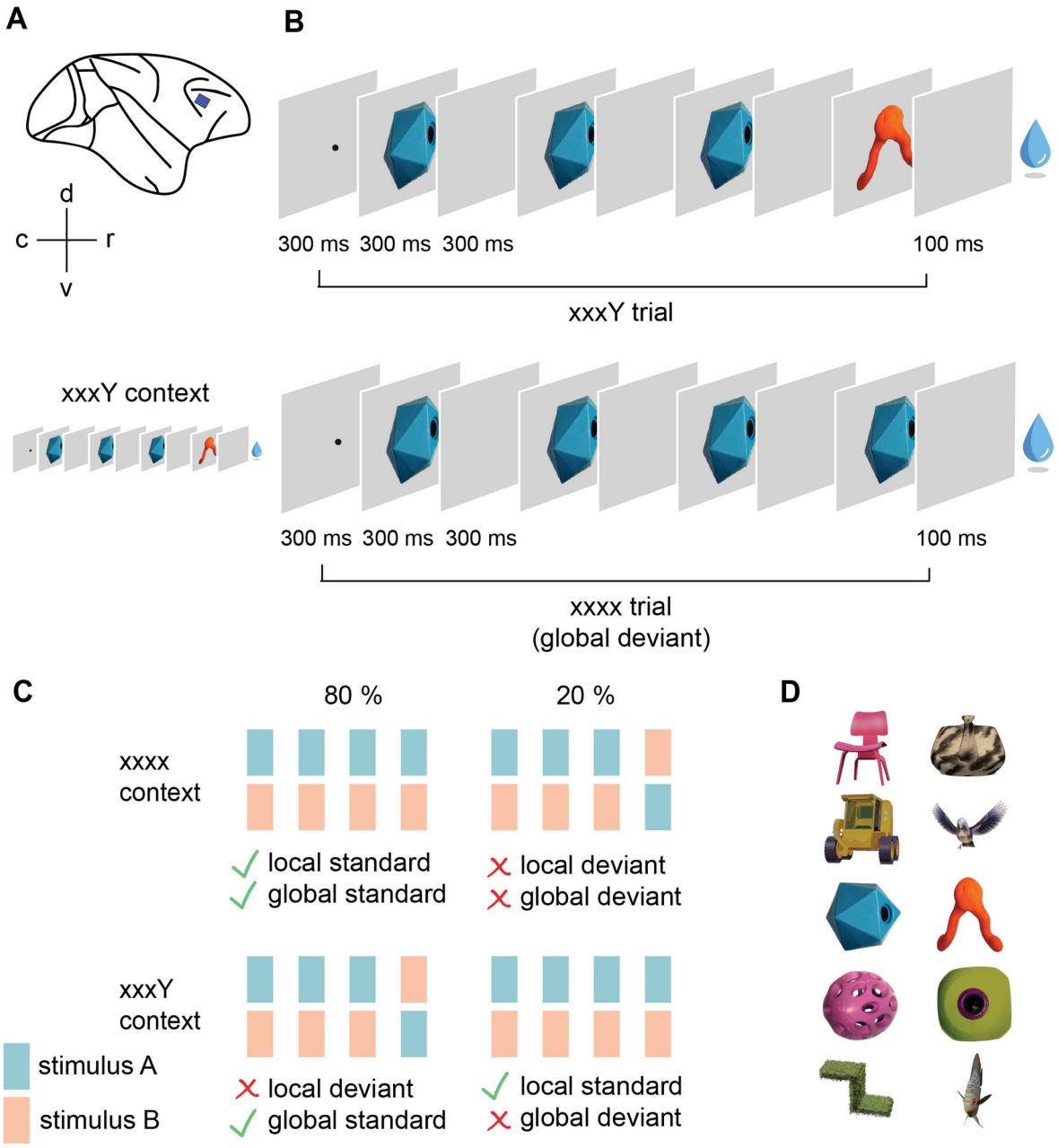

Figure 1. Recording vlPFC spiking activity during the visual local-global paradigm. A: Implantation of a Utah array in the macaque vlPFC. **B**: Example trials. On each trial, monkeys fixated for 300 ms prior to sequence onset. A sequence of 4 stimuli was presented with an SOA of 600 ms. 100 ms after offset of the last stimulus, the monkeys received a liquid reward. Examples show a single xxxY and an xxxx trial within the context of frequent xxxY sequences. **C**: Each session consisted of 4 blocks comprising a frequent sequence (global standard, which could have the structure xxxx or xxxY) and a rare sequence (global deviant). In a given block, the x was a fixed image (A or B, taken from the pairs in panel D) and the Y was the other image (B or A). A block consisted of 200 completed trials. The first 50 trials served as habituation to the global standard sequence (100% of trials), and then we presented a random mixture of 80% global standards and 20% global deviants, which differed only in the identity of the last item. The identity of A and B varied between recording sessions. **D**: The five pairs of visual stimuli (rows) used in the experiments.

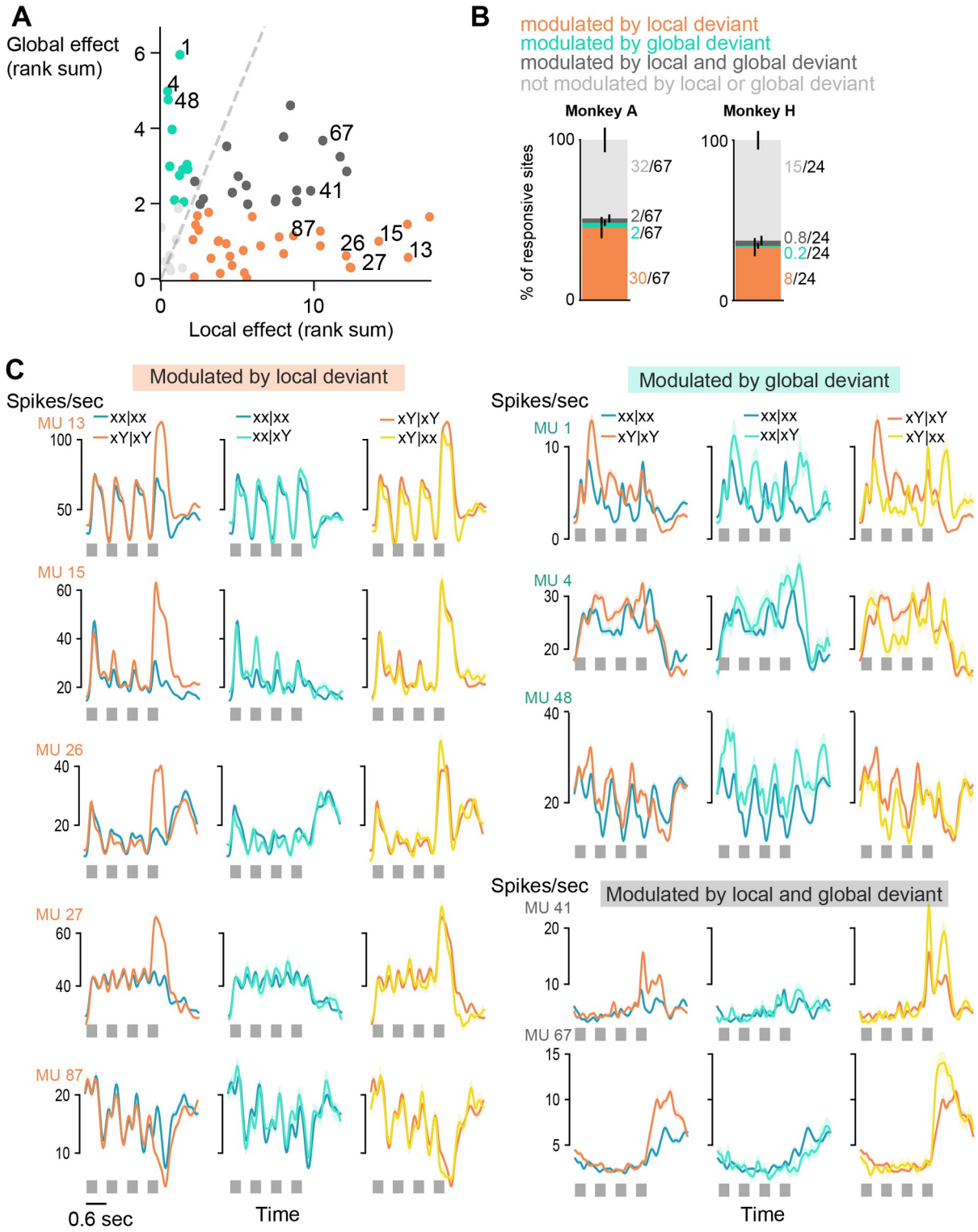

Figure 2. Modulation of spiking activity by local and global sequence structure at individual recording sites. A: Effect of local and global deviants (rank sum statistic, $p<0.05$ prior to correction for multiple comparisons) in task-responsive recording sites (dots) during one session in monkey A. Sites were significantly modulated by local (orange) or global (cyan) deviance only, by both local and global deviance (dark gray) or were not modulated by any deviance (light gray). The dashed gray line indicates equal magnitude of the effect of local and global deviance. **B**: The stacked bar graphs illustrate the proportion of task-responsive sites significantly modulated by local and / or global deviance (67 sites over 6 sessions in monkey A; 24 sites over 10 sessions in monkey H; Mann-Whitney U test with correction for multiple comparisons). Numbers next to the

graph correspond to the average number of sites across sessions per condition and error bars (centred on the stacked average proportions across sessions) indicate +- SD of the proportion. **C**: PSTHs of example MUA for sites plotted in **A**. Spiking activity was smoothed using a gaussian kernel with an SD of 50 ms. Colors indicate trial types, averaged over sequences with the A or B image identity. The “pure” local effect is shown by contrasting frequent xx (blue) and frequent xY trials (orange), the “pure” global effect by contrasting between rare vs. frequent xx trials (cyan vs. blue) and the effect of unpredicted over predicted local deviance is shown by contrasting rare vs. frequent xY trials (yellow vs. orange).

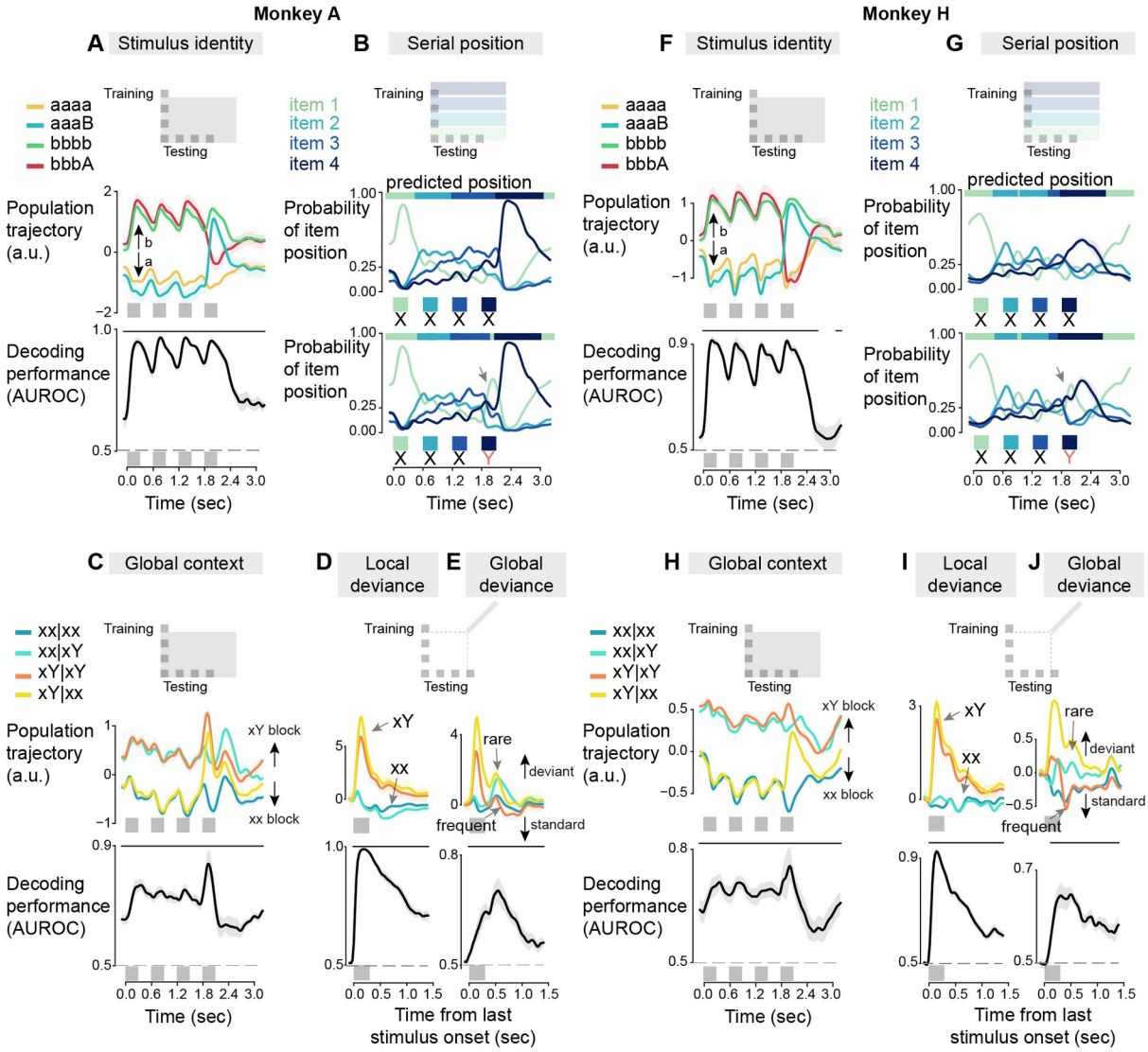

Figure 3. Decoding neural population codes for different aspects of the sequences. Multivariate linear regression was used to estimate the neural population vectors encoding stimulus identity, ordinal number, global context, local deviance and global deviance. The upper plots in all panels (and lower plot in B and G) show the neural trajectories, i.e. the MUA projected onto the population vectors resulting from the regression (with the time window used for training indicated in the inserts). Black traces in the bottom plots show decoder performance in terms of AUROC, relative to chance level 0.5. Horizontal lines on top of each graph indicate the time points for which the decoding performance was significantly above chance ($p<0.05$). Data from monkey A (left) and monkey H (right).

A, F: Decoding of image identity (picture A versus picture B). **B,G**: Decoding of the four ordinal positions in the sequence; the colored curves show the predictive probability of decoders which were trained on xx trials and generalized to xY trials. Note how the population activity in response to the local deviant resembled the response to the first item in a sequence. **C,H**: Decoding of global context, i.e. xY blocks versus xx blocks. Note how the decoding is significant even prior to sequence presentation, indicating an anticipation of the forthcoming sequence). **D,I**: Decoding of local deviance, i.e. xx versus xY sequences. **E,J**: Decoding of global deviance, i.e. frequent versus rare sequences. In panels **D,I,E,J** only, decoding was time-locked to the last sequence item (-100 ms to 1400 ms relative to last stimulus onset). A positive activation indicates a local or global deviance signal, respectively.

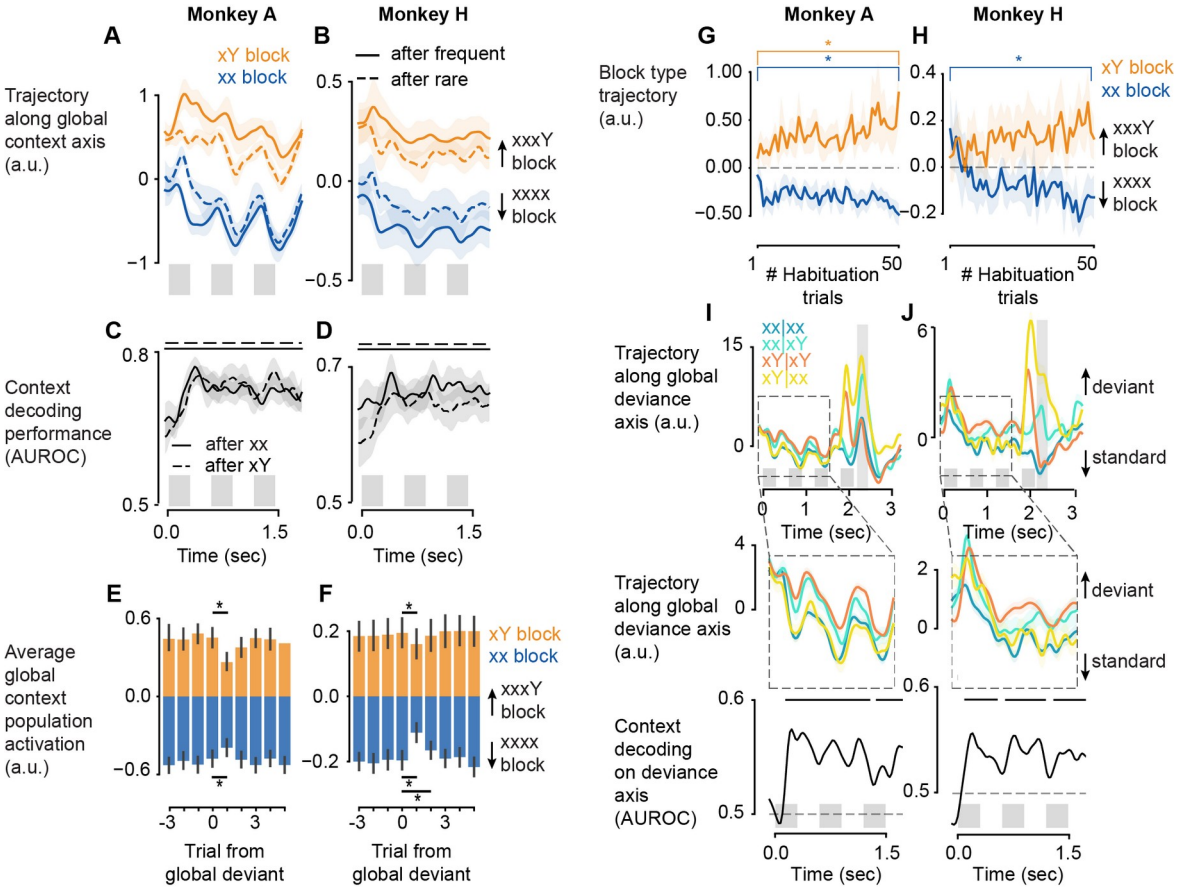

Figure 4. Neural signals reflecting the updating of global sequence knowledge. A,B: Population activity projected onto the axis coding for global sequence knowledge, i.e. xY blocks (orange) versus xx blocks (blue). Dashed curves indicate a reduction in the neural separation of xY and xx blocks after a rare global deviant. **C,D**: In both blocks, the global context can still be decoded after a global deviant trial (after xx trials in xY blocks and after xY trials in xx blocks), i.e. when the previous trial is suggestive of the opposite block. **E,F**: Activation of the global context axis averaged over the first three stimuli in each trial, aligned to rare trials in xY blocks (orange) or xx blocks (blue). Height of bars indicate average across trials from pooled sessions and error bars are the 95% CI. The asterisks denote a significant change in global context signal between the trial before the global deviance occured (0) and the following trial ($p<0.05$, paired t-test). **G,H**: Buildup of sequence knowledge during habituation. The neural activity during the 50 habituation trials of each block was projected onto the population axis that encoded global context and averaged over the first three stimuli in each trial. The asterisk denotes a significant difference ($p<0.05$) between the first and last habituation trial in a paired t-test across 14 blocks in monkey A and 20 blocks in monkey H (i.e. two blocks of each type per session). **I,J**: Trajectories of the neural population that leads to maximal overall global deviance decoding performance (Fig. 3E,J), indicated by the gray shaded area. The middle panel shows a zoom into the time period prior to the onset of the last stimulus and the bottom panel is the quantification of the context-decoding performance based on the activation of the global deviance population. Time periods of significant context decoding are indicated by the horizontal bars on top of the AUROC plots. The horizontal dashed line shows the chance level. Only trials following a global standard sequence were used. Curves indicate average across all trials from all sessions and shaded areas are +-sem.

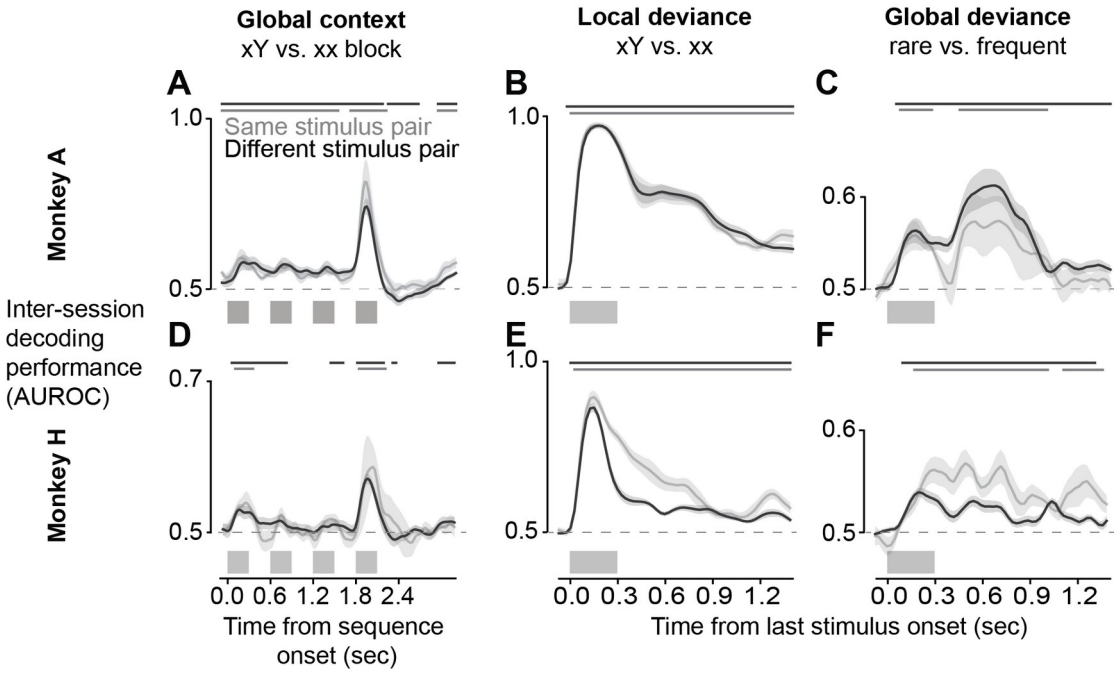

Figure 5. The population responses to global context, local deviance, and global deviance generalize to new sessions and stimuli. Plots show the generalization of decoding to new sessions with either the same visual stimuli (gray curve) or difference stimuli (black curve). Generalization performance (AUROC) is shown separately for decoders trained on global context (**A,D**), local deviance (**B,E**) and global deviance (**C,F**). Horizontal lines on top of each graph show time points where the decoding performance was significantly above chance ($p<0.05$).

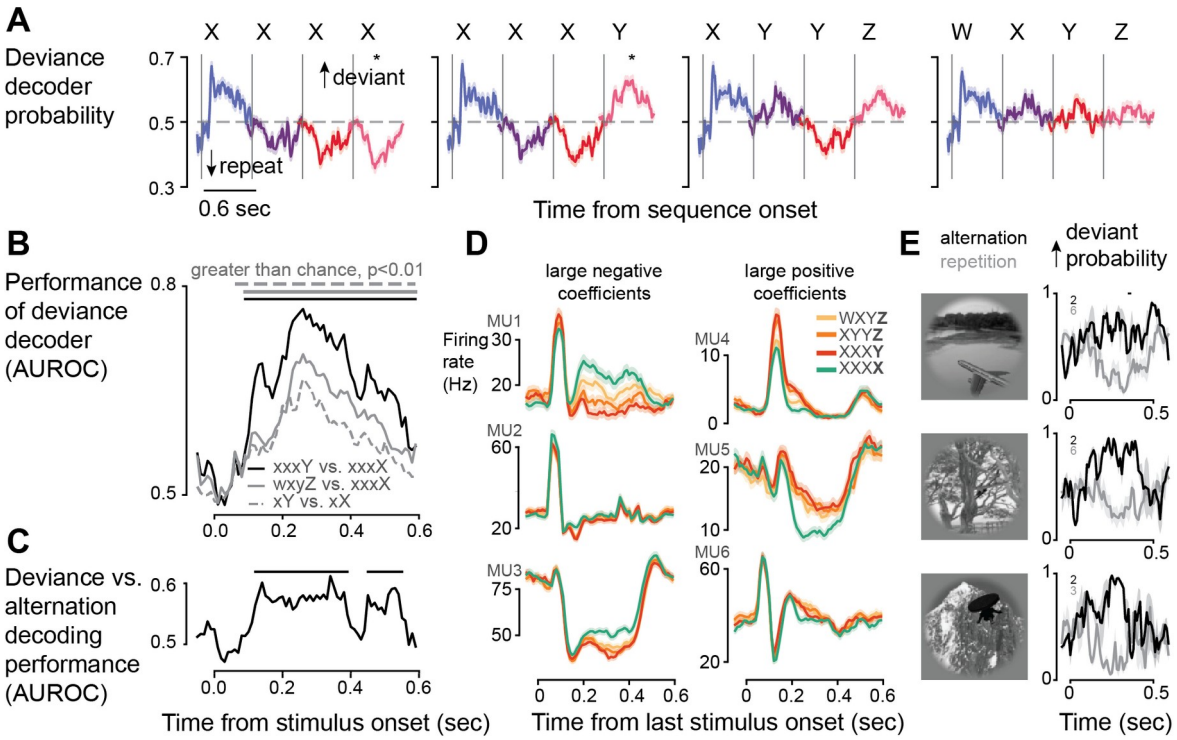

Figure 6. Abstract change and deviance detection by neural populations in monkey A. In a control experiment in monkey A, 4 possible sequence chunks (see titles in **A**) were presented in a uniform random manner. Letters W-Z indicate any of 948 grayscale images from the Brainscore database (Majaj et al., 2015), changing randomly in each trial. A neural decoder for local deviance was trained on XXXY vs. XXXX trials, indicated by the star in **A**, using leave-one-stimulus-out cross-validation. **A**: Predictive probability of the decoder for all sequence types and stimulus positions in a sequence (indicated by colors). **B**: Decoding performance in terms of AUROC for local deviants (XXXY vs. XXXX, black), novel stimulus, as well versus pure repeats (WXYZ vs. XXXX, gray), or any transition versus single repeats (XY vs. XX, dashed gray). All conditions could be decoded above chance level with $p<0.01$ (random permutation test). Horizontal bars indicate significant time bins. **C**: Rare stimuli that violate a local pattern of repetitions (XXXY) yielded a significantly higher response of this population than rare stimuli without preceding regularity (WXYZ), again indicated by horizontal bars on top. **D**: Examples of multi-units contributing to the population axis coding for local deviance. A large negative (left) or positive (right) coefficient means a lower, or higher firing rate for deviant stimuli, respectively. **E**: Population deviance response to repeats (light gray) or alternations (black) of three example images. Lines show mean across N number of trials (indicated by small numbers in each plot) and shaded areas show +- sem.

Sequence (one trial)	**Global context***	**Local deviance**	**Global deviance**	**Terminology**
xxxx (aaaa, bbbb)	xx block xY block	standard standard	standard deviant	xx|xx (frequent xx) xx|xY (rare xx)
xxxY (aaaB, bbbA)	xx block xY block	deviant deviant	deviant standard	xY|xx (rare xY) xY|xY (frequent xY)

Table 1: Terminology of sequence types in the local-global paradigm. *The global context corresponds to the structure of the frequent trials in a block. xx is short for a xxxx trial and xY is short for a xxxY trial. Colors indicate the color code used in Figures 2-4.

METHODS

Data and code availability

Code and data will be made publicly available upon publication.

EXPERIMENTAL MODEL AND SUBJECT DETAILS

Two adult rhesus macaques (A and H, 9 - 10 kg, 19 and 16 years old, respectively) participated in this study. Both animals were pair-housed. They had previously been implanted with a custom made skull-form-specific titanium headpost and trained on a passive visual fixation task with liquid reward in a primate chair. Daily water access was controlled during the experimental period. All procedures were conducted in accordance with the European convention for animal care (86-406) and the National Institutes of Health's Guide for the Care and Use of Laboratory Animals. Animal studies were approved by the institutional Ethical Committee (CETEA protocol #A18_028).

METHOD DETAILS

Sequence paradigm

An adaptation of the local-global paradigm (Bekinschtein et al., 2009) with visual stimuli was used. The stimuli were 10 colored images of objects, matched in luminance (Fig. 1D). Fixed pairs of images were used in every experiment, here denoted as stimulus A and B. The paradigm consisted in the presentation of binary visual sequences composed of 4 items. Each item was displayed for 300 ms, with an inter-stimulus interval (isi) of 300 ms (stimulus onset asynchrony, SOA - 600ms). The sequence could be one of four: aaaa or bbbb, denoted as xxxx; and aaaB or bbbA, denoted as xxxY, where the capital letter indicates a *local deviant*

item. One sequence was presented per trial which were organized in blocks of 200 trials. During each block, one sequence was used as the frequent, global standard sequence which was established during 50 habituation trials at the beginning of the block. 80% of the remaining 150 trials were global standards and 20% were global deviants, which differed in the last position compared to the standard. Each of the four sequence types was used as the global standard sequence in one block. We will denote a global context according to its global standard sequence: xxxx block for aaaa-frequent and bbbb-frequent or xxxY block for aaaB-frequent and bbbA-frequent. We will furthermore denote trials according to their context: xY|xx indicates a trial with a local deviant that occurs in a block of frequent xxxx sequences. The four trial types are thus xx|xx, xY|xY (global standards) and xx|xY, xY|xx (global deviants).

This two-by-two design enabled us to study effects of lower-order (local) and higher-order (global) sequence regularity. Consider for instance a single xxxY sequence: it ends with a local deviant, an image that violates the repeated structure of the previous three images. However, assuming that monkeys quickly detected the global sequence regularity in a block, the same local deviant, occurring within a block of similar xY global standard trials, is predictable and may no longer generate a global surprise (xY|xY, “predicted local deviant”). Conversely, a rare xx trial, which does not violate the local context, may elicit a global surprise when presented among many xY sequences (xx|xY, hereafter called “pure global deviant”).

Each trial started with the display of a black fixation spot (diameter of 0.3 degree) at the center of the screen. After 300 ms of fixation by the monkey, the fixation point disappeared and the sequence was displayed centrally with stimuli at a size

of 8 degrees per visual angle. The animals had to maintain the gaze within a window of 8 degrees of visual angle centered on the stimulus. A liquid reward was given for trial completion 100 ms after offset of the last item.

For monkey H, 5 stimulus pairs were used during a total of 10 experiments and for monkey A, 4 stimulus pairs were used during a total of 7 experiments.

Repetition versus change control experiment

We performed two sessions of an additional experiment with monkey A during which we showed four different types of sequence chunks containing each 4 images. The types of sequences were XXXX, XXXY, XYYZ and WXYZ, where letters indicate any of 948 grayscale images of objects from the Brainscore database (Majaj et al., 2015), randomly changing with each sequence presentation. Sequence types were uniformly distributed across a recording session so that there was no global context. All stimuli could occur in any position and were presented 1 to 5 times. This experiment served to control for stimulus-specific adaptation that could underly the deviance response to the last stimulus in XXXY trials. As we used a broad range of stimuli, the images used as WXY are expected to be on average as distant from Z than X is from Y in XXXY trials, thereby leading to the same amount of stimulus-specific adaptation for the population responding to Y (in XXXY) as to Z in (WXYZ).

The timing of the stimuli were the same as in the local-global experiment and the reward was given at 100 ms after offset of the last stimulus.

Implantation of microelectrode arrays

The macaques were tranquilized in their cage by intramuscular injection of ketamine 1000 (3 mg/kg) and dexmedetomidine (0.015 mg/kg). Once in the operating room, they were placed in a stereotactic frame and deeply anaesthetized (assisted respiration) by inhalation of oxygen (20%) and sevoflurane (1.5 -2%). An intravenous catheter was installed for the administration of physiological fluids (NaCl with 5% glucose, 10 ml/kg/h). A steroidal anti-inflammatory drug, the methylprednisolone (solumedrol 1 mg/kg i.m.) or dexamethasone (dexazone 0,5 mg/kg i.m.) is administered to prevent swelling of the cortex. As well as, an antibiotic (cefazoline 50 mg/kg i.m.) and a morphine derivative (buprecare 0.02 mg/kg i.m.). All surgical procedures were performed aseptically, and recordings of heart rate, respiration patterns, blood pressure and body temperature were monitored throughout the surgery.

Macaques were given a methylprednisolone (monkey A, 1 mg/kg) or dexamethasone dose (monkey H, 0.1 mg/kg) the day before the implantation to avoid brain edema. Monkey H received another dose of dexamethasone (0.5 mg/kg) the day of implantation. The implantation of the gas sterilized multielectrode array began with a longitudinal incision in the skin. The skin and underlying muscle was retracted and a craniotomy was performed over the lateral prefrontal cortex using a surgical drill. The bone flap was removed and then a U-shaped opening in the dura mater was made to expose the cortex. Hyperventilation after dura opening was used to reduce intracranial pressure and avoid swelling of the cortex. The Utah microelectrode array was implanted into the

inferior convexity of the prefrontal cortex, 1–2 mm anterior to the bank of the arcuate sulcus and below the ventral bank of the principal sulcus, using a pneumatic inserter (Blackrock Microsystems). The dimensions of the array was 4 × 4 mm in a 10 × 10 electrode configuration resulting in an electrode-to-electrode distance of 400 µm. The electrode length was 1 mm. The titanium connector that can be connected to the electrophysiological recording device was implanted on the skull with titanium screws. Then the dura mater was sewn back together, the bone flap was reinserted and secured by a thin titanium strip. Finally, the skin was sutured. After the electrode array implantation, injections of antibiotics (cefazoline 50 mg/kg i.m.) were given for 10 days and buprenorphine (0,015 mg/kg i.m.) for 3-5 days depending on the pain level.

QUANTIFICATION AND STATISTICAL ANALYSIS

Data preprocessing

The recorded broadband signals were preprocessed using Matlab. Broadband neural signals (0.1 - 30 kHz) were recorded with a Cerebus neural signal processor system (Blackrock Microsystems) and bandpass filtered offline between 0.6 - 3 kHz using a 2nd order Butterworth filter. Spikes were detected with an amplitude threshold set at five times the median absolute deviation and spike events larger than 50 times the mean absolute deviation were discarded. Further, spike events with an inter-spike interval of less than the refractory period of 0.5 ms

were also discarded. Spike times were aligned to the onset of the photodiode signal indicating the actual time of presentation of the last item in a sequence.

All further analyses were performed with Python. Firing rates of individual sites were computed from the spike times in non-overlapping bins of 25 ms and smoothed with a gaussian kernel corresponding to 50 ms standard deviation. For the data shown in Figure 6 and Suppl. Figure 5, firing rates were computed with a moving average window of 50 ms and a step size of 10 ms in order to obtain a better temporal resolution.

Single channel analyses

To quantify the modulation of single channel spiking activity by local and global deviance, we only considered recording sites that were significantly modulated by the task. As a criterion for task modulation, we tested if there was a difference in firing rate during the 300 ms fixation period prior to sequence onset and the first 300 ms after presentation of the last sequence stimulus. We used pairwise *t*-test per recording site and recording session and false discovery rate (FDR; Benjamini and Hochberg, 1995) across all sites and sessions within an animal to correct for multiple comparisons. Sites with a corrected p-value <= 0.05 were regarded as being modulated by the sequence task. We tested each of the task-modulated sites for effects of local and global deviance, using a Mann-Whitney-U test (Wilcoxon, 1945) on the average firing rate during 1 sec following the onset of the last stimulus, thus taking into account non-normal distribution of firing rates and substantially differing sample sizes in case of global deviants. For the summary of the results across recording sessions, we used FDR across tested sites and sessions per animal. A site with a corrected p-value <= 0.05 was regarded as

being modulated by the respective variable. For the scatter plot in Fig. 2A, FDR was not applied and colors indicate sites that have an uncorrected p-value of below 0.05, either for the global effect (cyan) or local effect (orange) only or independently for both effects (dark gray).

Population analyses

Multivariate linear regression

We assessed how the sequences were represented on the neural population level by computing the axes across the MUA space that carried most information about the variables *stimulus identity*, *global context*, *local* and *global deviance*, without pre-selection of recording sites. For this, we used multivariate linear regression, as in the subspace analysis in Mante et al. 2013. We performed two separate analyses, one to study the representation of the sequences prior to the last stimulus, and one for the time after onset of the last stimulus, in order to measure responses to deviants. For the time before the last stimulus onset, the variables stimulus identity and global context were considered, whereas the trial condition after onset of the last stimulus was defined by the variables stimulus identity, local and global deviance. As deviance responses following the last stimulus might be dynamic, we performed a separate regression per time bin between 0 until 1.4 sec after onset of the last stimulus.

The multivariate linear regression was performed separately for each recording channel with the above-mentioned sequence variables as independent variables and the MUA (*r*) of channel *i* (in a time bin *t*) as dependent variable:

$$r_{i,t} = \beta_{i,t}^{stimulus} \times stimulus + \beta_{i,t}^{local} \times local + \beta_{i,t}^{global} \times global + \varepsilon_{i,t} \quad (1)$$

The above equation holds for time bins *t* after presentation of the last stimulus. For the analysis of sequence structure representation before the last stimulus, the responses between 0 - 1.8 sec after sequence onset were averaged per trial and a single regression was performed per recording channel.

$$r_i = \beta_i^{stimulus} \times stimulus + \beta_i^{global\,context} \times global\,context + \varepsilon_i \quad (2)$$

$\boldsymbol{\varepsilon}$ is a noise parameter per channel (and time bin). *r* is a vector of dimension *Ntrials*, as are the independent variables stimulus, local, global and global context. Those were dummy variables, with A = -1, B = 1 for the stimulus variable; local or global standards = -1, local or global deviants = 1; xx block = -1 and xY block = 1. This approach results in a coefficient β per channel, variable, (and time bin) that indicates how much the firing of a channel was influenced by a certain variable.

The set of the 96 coefficients across all channels for one sequence variable *k* (and time point *t*) constitutes a 96-dimensional vector $^{(k)}$ (or $\boldsymbol{\beta}^{(k)}_t$) that we denote as the population axis representing this sequence variable. Note that Mante et al. 2013 orthogonalized these axes and denoised them using principal component analysis. We chose not to add these steps after regression in order to measure orthogonality resulting directly from the regression and because the data did not require further denoising.

Decoding from the population trajectories

In order to use the resulting population axes for decoding, the MUA of all channels was projected onto the population axis of each sequence variable *k*, respectively.

$$r_{j,t}^{(k)} = r_{j,t} \cdot \beta^{(k)} \quad (3)$$

or

$$r_{j,t}^{(k)} = r_{j,t} \cdot \beta_t^{(k)} \quad (4)$$

for time-varying population axes.

j is the trial index. r_j is a 96-dimensional vector of the population firing rate in a single trial *j* and time bin *t*. $r_{j,t}$ is a scalar and corresponds to the dimensionality-reduced population activity in one trial *j* and time bin *t* in the subspace carrying most information about a sequence variable *k*. This trial-by-trial projection was then used to classify trials according to each sequence variable. The sign of these projections was dependent on the definition of the independent variables (see above). A positive activation along the axis coding of stimulus identity, e.g., corresponded to stimulus B, whereas a negative activation corresponded to stimulus A. As a measure of decoding performance, we computed the area under the ROC curve (AUROC) by varying the decision boundary for classification.

Cross-validation

The decoding performance was cross-validated both within and across sessions. Within each session, we used 10-fold cross-validation, meaning that 90% of all data was included for the regression and the remaining 10% for projecting test data onto the obtained axes. This was repeated 10 times so that all trials were used for testing. We shuffled the data prior splitting and ensured a balance of trial conditions in the training data. The reported performance within a session is the AUROC across all tested trials.

For the cross-validation across sessions for the variables *global context, local and global deviance*, we used the population axes from one random training fold of

each session and projected all trials from all other sessions onto these axes. We then computed the AUROCs for each pair of training and test sessions and reported the performance separately for pairs that had the same or different stimulus pairs.

Decoding of serial position

We used multinomial logistic regression to predict the item position in a sequence based on the neural population responses. This was a classification with 4 target classes (item 1-4). The 300 ms after onset of a stimulus, shifted by 100 ms, were labelled with the item number of the most recent stimulus. The activity of each channel was averaged in these intervals, resulting in 4 values per trial. The 4 items from all trials were pooled and used to train the classifiers, using 10-fold cross-validation. Only xx trials were used for training. For testing, the activity in each test trial and time bin between 100 ms prior to sequence onset until 1.4 sec after sequence offset was passed through the trained classifier. This resulted in predictive probabilities for item 1 to 4 over time and allowed us to study the dynamic encoding of item position throughout a trial. We also assessed item position classification on incomplete trials. The monkeys could break fixation at any time during a trial by moving the gaze outside of the 6 degree fixation window which aborted the presentation of the sequence. We computed the predictions for item position 1 to 4 for trials interrupted after presentation of the first, second or third stimulus. Note that the fixation break could have occurred at any time between onset of one stimulus and onset of the next stimulus, meaning that the time the monkeys perceived the last stimulus varied within one condition.

Cross-condition decoding of global deviance

To test for encoding of global deviance irrespective of local deviance, we trained a separate binary classifier to predict global deviance for the time after last stimulus onset, on xx trials only and tested on xY trials. We used logistic regression on the pooled data from all sessions, per animal. This was done to reduce the impact of the block structure of the task within each session, which could have been problematic in this case, as the classifier was trained from global deviants and standards from separate blocks (e.g. rare xx in an xY block vs. frequent xx in an xx block). Decoding performance was again measured as AUROC for each time bin, separately for each session.

Decoding of deviance or change in control data

We used logistic regression to predict whether a sequence chunk was XXXY or XXXX (deviance decoder), based on the activity after the last stimulus. We used a time-varying decoder in time bins of 50 ms, and with a step size of 10 ms. Image identities were balances in both conditions, i.e. we only included stimuli for training that occured in XXXY and XXXX chunks, resulting in 757 unique images. Decoder performance was cross-validated by leaving trials with one image out for testing. We hence trained 757 different classifiers. Images that did not occur in both conditions (191 different images) were only used once for testing but not included in the training set.

We additionally trained a decoder to detect any change from a repetition by contrasting the response to alternations and repeats in the second and third position of sequence chunks (i.e. the second stimulus in WXYZ and XYYZ trials vs. the second stimulus in XXXY trials as well as the third stimulus in WXYZ vs.

the third stimulus in XYYZ trials). The same cross-validation approach was used to test this decoder.

Assessment of learning effects during the habituation period

We measured whether the code for global context evolved over the course of the habituation period. For this, we projected the activity of single habituation trials (0 - 1.6 seq after sequence onset) onto the population vector that separated xx from xY blocks during the test trials within the same session. As we had used 10-fold cross-validation to obtain those vectors, we also obtained 10 projections of the same habituation trials. We averaged those projections across folds to obtain one activation value for the global context trajectory per trial. To assess learning, we tested the difference in the activation during the first trial vs. the 50th trial using a paired t-test with N=14 blocks in monkey A and N=20 blocks in monkey H. This was done separately for xx and xY blocks, assuming that xx blocks would show an evolution towards a more negative activation (which was defined as the xx block direction) and xY blocks an evolution towards a more position activation (xY block direction).

Random permutation test

To test the significance of decoding performance from population trajectories, we used a random permutation test with cluster-based correction for multiple comparisons (Maris and Oostenveld 2007). After estimating the population axes and projecting single trials onto these axes, we generated 100 surrogate datasets by shuffling the trial conditions of test trials. We then computed the AUROCs for the different sequence variables based on the trajectories with the shuffled trial

labels. We averaged the true AUROCs across recording sessions (10 in monkey H, 7 in monkey A) and likewise obtained 100 surrogate session-averages. The true AUROCs per sequence variable were transformed into t-values by subtracting the average over the permutations and dividing by their standard deviation, separately for each time point. Absolute t-scores that passed a threshold of 3 standard deviations were candidates for significant clusters in time. A correction for multiple comparisons across time was performed by comparing the sum of t-values within each true cluster with the sum of t-values within surrogate clusters. Those surrogate clusters were obtained by transforming each of the 100 permutation samples into t-values by subtracting the mean of the remaining 99 samples and dividing by their standard deviation. If a true cluster had a sum of absolute t-values larger than 95% of the largest surrogate clusters, it passed the threshold for significance which was set to a type-1 error of 5%. For the test of decoding performance across sessions, the same procedure was followed. First, we averaged for each test session the performance based on the decoder trained on the different possible training sessions (same or different stimulus pair). Second, we averaged the 10 or 7 test sessions. The same was done for the surrogate AUROCs based on shuffled trial labels.

The same test was also performed for the cross-condition decoding of global deviance and the effect of deviance onto eye movements (see below).

Analysis of eye movements

The eye velocity (v) was measured from the non-calibrated horizontal (x) and vertical (y) eye position recording by computing the difference between time bins (t).

$$v_t = | x_t - x_{t-1} | + | y_t - y_{t-1} | \quad (5)$$

To test for an effect of local or global novelty on eye movements, the median smoothed velocity (20 ms moving average) in each condition was computed across trials from all sessions and tested using a random permutation test (see above). We then controlled for eye movements in the time window during which there was a significant effect of deviants, +- 100 ms to be more inclusive, by removing deviant trials with an average velocity in this time period above the median eye velocity in the standard trials. The effect of deviance in the neural data was visualized for all trials vs. the controlled case (Fig. S5).

References

Auksztulewicz, R., & Friston, K. (2016). Repetition suppression and its contextual determinants in predictive coding. Cortex, 80, 125-140.Auksztulewicz, R., and Friston, K. (2016). Repetition suppression and its contextual determinants in predictive coding. Cortex.

Baeg, E.H., Kim, Y.B., Huh, K., Mook-Jung, I., Kim, H.T., and Jung, M.W. (2003). Dynamics of Population Code for Working Memory in the Prefrontal Cortex. Neuron *40*, 177–188.

Basirat, A., Dehaene, S., and Dehaene-lambertz, G. (2014). A hierarchy of cortical responses to sequence violations in three-month-old infants. Cognition *132*, 137–150.

Bastos, A.M., Usrey, W.M., Adams, R.A., Mangun, G.R., Fries, P., and Friston, K.J. (2012). Canonical Microcircuits for Predictive Coding. Neuron *76*, 695–711.

Bekinschtein, T.A., Dehaene, S., Rohaut, B., Tadel, F., Cohen, L., and Naccache, L. (2009). Neural signature of the conscious processing of auditory regularities. PNAS *106*, 1672–1677.

Brainard, D.H. (1997). The Psychophysics Toolbox. Spatial Vision *10*, 433–436.

Carbajal, G.V., and Malmierca, M.S. (2018). The Neuronal Basis of Predictive Coding Along the Auditory Pathway: From the Subcortical Roots to Cortical Deviance Detection. Trends in Hearing *22*.

Casado-Román, L., Carbajal, G.V., Pérez-González, D., and Malmierca, M.S. (2020). Prediction error signaling explains neuronal mismatch responses in the medial prefrontal cortex. PLoS Biology *18*, 1–29.

Chao, Z.C., Takaura, K., Wang, L., Fujii, N., and Dehaene, S. (2018). Large-Scale Cortical Networks for Hierarchical Prediction and Prediction Error in the Primate Brain. Neuron *100*, 1252-1266.e3.

Dehaene, S., and Changeux, J.P. (2011). Experimental and Theoretical Approaches to Conscious Processing. Neuron.

Dehaene, S., Kerszberg, M., and Changeux, J.-P. (1998). A neuronal model of a global workspace in effortful cognitive tasks. PNAS *95*, 14529–14534.

Dehaene, S., Meyniel, F., Wacongne, C., Wang, L., and Pallier, C. (2015). The Neural Representation of Sequences: From Transition Probabilities to Algebraic Patterns and Linguistic Trees. Neuron *88*, 2–19.

Deouell, L.Y. (2007). The Frontal Generator of the Mismatch Negativity Revisited. Journal of Psychophysiology *21*, 188–203.

Donahue, C.H., and Lee, D. (2015). Dynamic routing of task-relevant signals for decision making in dorsolateral prefrontal cortex. Nat Neurosci *18*, 295–301.

Dürschmid, S., Edwards, E., Reichert, C., Dewar, C., Hinrichs, H., Heinze, H.-J., Kirsch, H.E., Dalal, S.S., Deouell, L.Y., and Knight, R.T. (2016). Hierarchy of prediction errors for auditory events in human temporal and frontal cortex. PNAS *113*, 6755–6760.

Dürschmid, S., Reichert, C., Hinrichs, H., Heinze, H.-J., Kirsch, H.E., Knight, R.T., and Deouell, L.Y. (2019). Direct Evidence for Prediction Signals in Frontal Cortex Independent of Prediction Error. Cerebral Cortex *29*, 4530–4538.

Ebitz, R.B., and Hayden, B.Y. (2021). The population doctrine in cognitive neuroscience. Neuron *0*.

El Karoui, I., King, J.R., Sitt, J., Meyniel, F., Van Gaal, S., Hasboun, D., Adam, C., Navarro, V., Baulac, M., Dehaene, S., et al. (2015). Event-related potential, time-frequency, and functional connectivity facets of local and global auditory novelty processing: An intracranial study in humans. Cerebral Cortex *25*, 4203–4212.

Euler, M.J. (2018). Intelligence and uncertainty: Implications of hierarchical predictive processing for the neuroscience of cognitive ability. Neuroscience & Biobehavioral Reviews *94*, 93–112.

Fishman, Y.I., and Steinschneider, M. (2012). Searching for the mismatch negativity in primary auditory cortex of the awake monkey: Deviance detection or stimulus specific adaptation? Journal of Neuroscience *32*, 15747–15758.

Friston, K. (2005). A theory of cortical responses. 815–836.

Friston, K. (2010). The free-energy principle: a unified brain theory? Nat Rev Neurosci *11*, 127–138.

Friston, K. (2018). Does predictive coding have a future? Nat Neurosci *21*, 1019–1021.

Fujii, N., and Graybiel, A.M. (2003). Representation of action sequence boundaries by macaque prefrontal cortical neurons. Science *301*, 1246–1249.

Garrido, M.I., Kilner, J.M., Stephan, K.E., and Friston, K.J. (2009). The mismatch negativity: A review of underlying mechanisms. Clinical Neurophysiology *120*, 453–463.

Gil-da-Costa, R., Stoner, G.R., Fung, R., and Albright, T.D. (2013). Nonhuman primate model of schizophrenia using a noninvasive EEG method. PNAS *110*, 15425–15430.

Hamm, J.P., Shymkiv, Y., Han, S., Yang, W., and Yuste, R. (2021). Cortical ensembles selective for context. Proceedings of the National Academy of Sciences *118*.

Kaliukhovich, D.A., and Vogels, R. (2014). Neurons in Macaque Inferior Temporal Cortex Show No Surprise Response to Deviants in Visual Oddball Sequences. J. Neurosci. *34*, 12801–12815.

Kapoor, V., Besserve, M., Logothetis, N.K., and Panagiotaropoulos, T.I. (2018). Parallel and functionally segregated processing of task phase and conscious content in the prefrontal cortex. Commun Biol *1*, 1–12.

Kapoor, V., Dwarakanath, A., Safavi, S., Werner, J., Besserve, M., Panagiotaropoulos, T.I., and Logothetis, N.K. (2020). Decoding the contents of consciousness from prefrontal ensembles.

Kim, J.N., and Shadlen, M.N. (1999). Neural correlates of a decision in the dorsolateral prefrontal cortex of the macaque. Nature Neuroscience *2*, 176–185.

Levinson, M., Podvalny, E., Baete, S.H., and He, B.J. (2021). Cortical and subcortical signatures of conscious object recognition. Nat Commun *12*, 2930.

Majaj, N.J., Hong, H., Solomon, E.A., and DiCarlo, J.J. (2015). Simple Learned Weighted Sums of Inferior Temporal Neuronal Firing Rates Accurately Predict Human Core Object Recognition Performance. J. Neurosci. *35*, 13402–13418.

Mante, V., Sussillo, D., Shenoy, K.V., and Newsome, W.T. (2013). Context-dependent computation by recurrent dynamics in prefrontal cortex. Nature *503*, 78–84.

Markowitz, D.A., Curtis, C.E., and Pesaran, B. (2015). Multiple component networks support working memory in prefrontal cortex. PNAS *112*, 11084–11089.

May, P.J.C., and Tiitinen, H. (2010). Mismatch negativity (MMN), the deviance-elicited auditory deflection, explained. Psychophysiology *47*, 66–122.

Meirhaeghe, N., Sohn, H., and Jazayeri, M. (2021). A precise and adaptive neural mechanism for predictive temporal processing in the frontal cortex. Neuron *109*, 2995-3011.e5.

Merten, K., and Nieder, A. (2012). Active encoding of decisions about stimulus absence in primate prefrontal cortex neurons. PNAS *109*, 6289–6294.

Meyer, T., and Olson, C.R. (2011). Statistical learning of visual transitions in monkey inferotemporal cortex. PNAS *108*, 19401–19406.

Meyer, T., Ramachandran, S., and Olson, C.R. (2014). Statistical Learning of Serial Visual Transitions by Neurons in Monkey Inferotemporal Cortex. J. Neurosci. *34*, 9332–9337.

Miller, E.K., and Cohen, J.D. (2001). An Integrative Theory of Prefrontal Cortex Function. Annual Review of Neuroscience *24*, 167–202.

Miller, E.K., Gochin, P.M., and Gross, C.G. (1991). Habituation-like decrease in the responses of neurons in inferior temporal cortex of the macaque. Visual Neuroscience *7*, 357–362.

Miller, E.K., Erickson, C.A., and Desimone, R. (1996). Neural Mechanisms of Visual Working Memory in Prefrontal Cortex of the Macaque. J. Neurosci. *16*, 5154–5167.

Moutard, C., Dehaene, S., and Malach, R. (2015). Spontaneous Fluctuations and Non-linear Ignitions: Two Dynamic Faces of Cortical Recurrent Loops. Neuron *88*, 194–206.

Näätänen, R., Gaillard, A.W.K., and Mäntysalo, S. (1978). Early selective-attention effect on evoked potential reinterpreted. Acta Psychologica *42*, 313–329.

Näätänen, R., Paavilainen, P., Rinne, T., and Alho, K. (2007). The mismatch negativity (MMN) in basic research of central auditory processing: A review. Clinical Neurophysiology *118*, 2544–2590.

Nieder, A. (2012). Supramodal numerosity selectivity of neurons in primate prefrontal and posterior parietal cortices. PNAS *109*, 11860–11865.

Nieder, A., and Merten, K. (2007). A Labeled-Line Code for Small and Large Numerosities in the Monkey Prefrontal Cortex. J. Neurosci. *27*, 5986–5993.

Panagiotaropoulos, T.I., Deco, G., Kapoor, V., and Logothetis, N.K. (2012). Neuronal Discharges and Gamma Oscillations Explicitly Reflect Visual Consciousness in the Lateral Prefrontal Cortex. Neuron *74*, 924–935.

Parras, G.G., Nieto-Diego, J., Carbajal, G.V., Valdés-Baizabal, C., Escera, C., and Malmierca, M.S. (2017). Neurons along the auditory pathway exhibit a hierarchical organization of prediction error. Nat Commun *8*, 2148.

Parthasarathy, A., Herikstad, R., Bong, J.H., Medina, F.S., Libedinsky, C., and Yen, S.-C. (2017). Mixed selectivity morphs population codes in prefrontal cortex. Nat Neurosci *20*, 1770–1779.

Pazo-Alvarez, P., Cadaveira, F., and Amenedo, E. (2003). MMN in the visual modality: A review. Biological Psychology *63*, 199–236.

Pelli, D.G. (1997). The VideoToolbox software for visual psychophysics: transforming numbers into movies. Spatial Vision *10*, 437–442.

Pinotsis, D.A., Buschman, T.J., and Miller, E.K. (2019). Working Memory Load Modulates Neuronal Coupling. Cerebral Cortex *29*, 1670–1681.

Rao, R.P.N., and Ballard, D.H. (1999). Predictive coding in the visual cortex: a functional interpretation of some extra-classical receptive-field effects. Nat Neurosci *2*, 79–87.

Rigotti, M., Barak, O., Warden, M.R., Wang, X.-J., Daw, N.D., Miller, E.K., and Fusi, S. (2013). The importance of mixed selectivity in complex cognitive tasks. Nature *497*, 585–590.

Ruhnau, P., Herrmann, B., and Schröger, E. (2012). Finding the right control: The mismatch negativity under investigation. Clinical Neurophysiology *123*, 507–512.

Saez, A., Rigotti, M., Ostojic, S., Fusi, S., and Salzman, C.D. (2015). Abstract Context Representations in Primate Amygdala and Prefrontal Cortex. Neuron *87*, 869–881.

Shalgi, S., and Deouell, L.Y. (2007). Direct evidence for differential roles of temporal and frontal components of auditory change detection. Neuropsychologia *45*, 1878–1888.

Siegel, M., Buschman, T.J., and Miller, E.K. (2015). Cortical information flow during flexible sensorimotor decisions. Science *348*, 1352–1355.

Stokes, M.G., Kusunoki, M., Sigala, N., Nili, H., Gaffan, D., and Duncan, J. (2013). Dynamic Coding for Cognitive Control in Prefrontal Cortex. Neuron *78*, 364–375.

Strauss, M., Sitt, J.D., King, J.-R., Elbaz, M., Azizi, L., Buiatti, M., Naccache, L., Wassenhove, V. van, and Dehaene, S. (2015). Disruption of hierarchical predictive coding during sleep. PNAS *112*, E1353–E1362.

Summerfield, C., and de Lange, F.P. (2014). Expectation in perceptual decision making: neural and computational mechanisms. Nat Rev Neurosci *15*, 745–756.

Summerfield, C., Egner, T., Greene, M., Koechlin, E., Mangels, J., and Hirsch, J. (2006). Predictive Codes for Forthcoming Perception in the Frontal Cortex. Science *314*, 1311–1314.

Summerfield, C., Trittschuh, E.H., Monti, J.M., Mesulam, M.M., and Egner, T. (2008). Neural repetition suppression reflects fulfilled perceptual expectations. Nature Neuroscience *11*, 1004–1006.

Todorovic, A., and Lange, F.P. de (2012). Repetition Suppression and Expectation Suppression Are Dissociable in Time in Early Auditory Evoked Fields. J. Neurosci. *32*, 13389–13395.

Uhrig, L., Dehaene, S., and Jarraya, B. (2014). A Hierarchy of Responses to Auditory Regularities in the Macaque Brain. J. Neurosci. *34*, 1127–1132.

Viswanathan, P., and Nieder, A. (2013). Neuronal correlates of a visual “sense of number” in primate parietal and prefrontal cortices. PNAS *110*, 11187–11192.

van Vugt, B., Dagnino, B., Vartak, D., Safaai, H., Panzeri, S., Dehaene, S., and Roelfsema, P.R. (2018). The threshold for conscious report: Signal loss and response bias in visual and frontal cortex. Science *360*, 537–542.

Wacongne, C., Labyt, E., Wassenhove, V. van, Bekinschtein, T., Naccache, L., and Dehaene, S. (2011). Evidence for a hierarchy of predictions and prediction errors in human cortex. Proceedings of the National Academy of Sciences *108*, 20754–20759.

Wacongne, C., Changeux, J.-P., and Dehaene, S. (2012). A Neuronal Model of Predictive Coding Accounting for the Mismatch Negativity. Journal of Neuroscience *32*, 3665–3678.

Wallis, J.D., Anderson, K.C., and Miller, E.K. (2001). Single neurons in prefrontal cortex encode abstract roles. Nature *411*, 953–956.

Walsh, K.S., McGovern, D.P., Clark, A., and O’Connell, R.G. (2020). Evaluating the neurophysiological evidence for predictive processing as a model of perception. Annals of the New York Academy of Sciences *1464*, 242–268.

Wang, L., Uhrig, L., Jarraya, B., and Dehaene, S. (2015). Representation of Numerical and Sequential Patterns in Macaque and Human Brains. Current Biology.

Watanabe, M., and Sakagami, M. (2007). Integration of Cognitive and Motivational Context Information in the Primate Prefrontal Cortex. Cerebral Cortex *17*, i101–i109.

Wilson, B., Marslen-Wilson, W.D., and Petkov, C.I. (2017). Conserved Sequence Processing in Primate Frontal Cortex. Trends in Neurosciences *40*, 72–82.

Winkler, I. (2007). Interpreting the Mismatch Negativity. Journal of Psychophysiology *21*, 147–163., 147–163.

Zhang, S., Xu, M., Kamigaki, T., Hoang Do, J. P., Chang, W. C., Jenvay, S., Miyamichi, K., Luo, L., & Dan, Y. (2014). Selective attention. Long-range and local circuits for top-down modulation of visual cortex processing. Science 345(6197), 660–665.